

Supplementary Information

Finely Regulated Quantum Well Structure in Quasi-2D Ruddlesden-Popper Perovskite Solar Cell with an Efficiency Exceeding 20%

Jianghu Liang,^a Zhanfei Zhang,^a Qi Xue,^a Yiting Zheng,^a Xueyun Wu,^a Ying Huang,^a Xin Wang,^a Chaochao Qin,^c Zhenhua Chen,^b and Chun-Chao Chen^{a*}

^aSchool of Materials Science and Engineering, Shanghai Jiao Tong University, Shanghai 200240, P. R. China

^bShanghai Synchrotron Radiation Facility (SSRF), Shanghai Advanced Research Institute, Chinese Academy of Sciences, Shanghai 201800, P. R. China

^cHenan Key Laboratory of Infrared Materials and Spectrum Measures and Applications, School of Physics, Henan Normal University, 453007 Xinxiang, P. R. China

Experiment Section

Materials

ITO glasses are customized by Liaoning Huite Optoelectronics Technology Co., Ltd. SnO₂ colloid precursor (tin(IV) oxide, 15% in H₂O colloidal dispersion) is obtained from Alfa Aesar. MACl, FAI, and MAI are obtained from Dyesol. PbI₂, 2-thiophenemethylammonium iodide (TMAI), phenylethylammonium iodide (PEAI), butylammonium (BAI), lithium bis(trifluoromethylsulfonyl) imide (Li-TFSI, 95%), and poly(triaryl amine) (PTAA) are purchased from Xi'an Polymer Light Technology. N,N-dimethylformamide (DMF, 99.8%), isopropanol (99.9%), 4-tert-butylpyridine (tBP, 96%), and chlorobenzene (99.9%) are obtained from Sigma-Aldrich. 2,2',7,7'-tetrakis-(N,N-di-pmethoxyphenylamine)-9,9'-spirobifluorene (Spiro-OMeTAD), and perovskite/[6,6]-phenyl C61-butyric acid methyl ester (PCBM) are purchased from

Lumtec, Taiwan. Poly(3,4-ethylenedioxythiophene):poly(styrenesulfonate) (PEDOT:PSS, PVP AI4083) was purchased from Heraeus Clevis and used as received. Other chemicals such as alcoholic solvents are obtained from Shanghai Aladdin Biochemical Technology Co., Ltd or Shanghai Macklin Biochemical Co., Ltd and are used directly without further purification. Other spacer cations such as 3TMAI, BTMAI, TEAI, and FPMAI are synthesized according to published works.¹

Device fabrication

ITO glass substrates are cleaned ultrasonically in detergent, deionized water, acetone, and isopropanol successively for 15 min. Prior to use, the ITO substrates are dried by N₂ flow and then treated with UV-ozone for 15 min. Then, the diluted SnO₂ colloid (2.67%, in water) is spin-coated onto ITO substrates at 3500 rpm for 30 s and annealed on a hot plate at 150 °C for 30 min. After cooling to room temperature, the ITO/SnO₂ substrates are treated with UV-ozone again for 15 min.

The perovskite layer is spin-coated onto the ITO/SnO₂ substrates by one-step deposition method. The precursor solution of perovskite is composed of TMAI (106.1mg), FAI (151.4 mg), MACl (60.6 mg), PbI₂ (507.1), and DMF (1 mL). This solution was heated and stirred at 60 °C for 2 hours, and then filtered with polytetrafluoroethylene (PTFE) filter (0.22 μm) before use. Then, 60 μL perovskite precursor solution was dropped onto ITO/SnO₂ substrate, which was spin-coated at 1000 rpm for 5 s with a ramping rate of 500 rpm/s, and 5000 rpm for 20 s with a ramping rate of 1000 rpm s⁻¹. At the 8th second before the end of the spin-coating program, 100 μL of isopropanol or other antisolvent was gently dropped onto the center of ITO/SnO₂ substrate. After dripping the antisolvent, the wet perovskite film is brown and transparent. Then the film was annealed at 105 °C for 30 min.

Next, Spiro-OMeTAD (72.3 mg mL⁻¹ in chlorobenzene) with the addition of Li-TFSI (54 mL, 170 mg mL⁻¹ in acetonitrile) and tBP (30 mL) is spin-coated at 3000 rpm. for 30 s. Finally, the Ag or Au back electrodes (100 nm) is deposited by thermal evaporation.

The film of iPA-MA is prepared by the same process described above, except that FAI in the precursor solution is totally substituted by MAI. The film of n=3 is prepared from

a precursor solution of TMAI:FAI:PbI₂:MACl=2:2:3:2. The same procedure described above is used to fabricate the film.

The 3D perovskite film was fabricated according to published work.² The composition in the precursor solution is FAI:PbI₂:MACl=2:2:1. The 2D capping layer is fabricated by spin coating a TMAI solution (20 mM in isopropanol) at 5000 rpm for 30 s on top of the 3D perovskite layer. Then the film is annealed at 100 °C for 5 min and scraped off to obtain a powder for ¹H NMR characterization.

Inverted device structure

A thin layer of poly(3,4-ethylenedioxythiophene):poly(styrenesulfonate) (PEDOT:PSS, 4083) was fabricated by spin-coated at 5000 rpm for 30 s in air and annealed at 150 °C for 30 min. The NiO_x layer, the PCBM layer, and the BCP layer were fabricated according our previous work.³ The fabrication process of 2D perovskite layer is the same as above.

Solubility test

The precursor solution was prepared by mixing the corresponding organic cations and an equal molar ratio of PbI₂ in DMF with a concentration of 1M (Pb²⁺). Then, 20 μL of antisolvent (iPA or nBA) was added into 300 μL above precursor solution each time, and the mixed solution was shaken vigorously. The critical volume of antisolvent required to precipitate the solution was recorded in **Table S2**.

Characterization

The current density–voltage (*J–V*) curves of the device was measured under AM1.5G illumination at 100 mW cm⁻² (calibrated with a standard Si solar cell) using an Abet Technologies Sun 2000 solar simulator and a Keithley 2400 source meter. The device was measured by reverse scan (1.2 V → -0.1 V, step 50 mV) and forward scan (-0.1 V → 1.2 V, step 50 mV) in ambient air (30% RH). External quantum efficiency (EQE) measurement was conducted on the QTEST HIFINITY 5 EQE system (the light intensity was calibrated with standard Si detectors). UV-vis absorption spectra were acquired on a Lambda 35 UV-vis spectrometer. Steady state photoluminescence (PL) spectra and time-resolved photoluminescence (TRPL) spectra and external

photoluminescence quantum efficiency (PLQE) were taken on an FLS1000 photoluminescence spectrometer with an excitation wavelength of 470 nm. The adjustment of the fluence of laser in the fluence-dependent TRPL decay experiment is achieved through a neutral density filter. During the PLQE measurement, the excitation wavelength is 535 nm, and an integrating sphere setup is used. The external PLQE value is calculated as per de Mello et al.⁴ Confocal laser scanning microscopy photoluminescence (CLSM-PL) images were acquired on LSM 900 with Airyscan 2 under ambient air condition. X-ray diffraction (XRD) patterns were acquired on D8 Advance X-ray diffractometer with Cu K α radiation as the X-ray source with a scan rate of 6° min⁻¹. Field emission scanning electron microscopy (FE-SEM) images were acquired on TESCA MIRA3 FE-SEM. Kelvin probe force microscopy (KPFM) and AFM images were taken by Bruker Bio-FastScan AFM. TEM images were acquired from Talos F200X G2, the TEM sample was prepared by scraping quasi-2D perovskite films from ITO substrates and dispersed in chloroform. Then, a carbon support film was immersed into above suspension liquid for 1 s for TEM measurement. Ultraviolet photoelectron spectra (UPS) were measured by Thermo Fisher ESCALAB 250Xi under excitation from the He I line (21.22eV) of a helium discharge lamp. Electrochemical impedance spectroscopy (EIS) spectra were obtained by Chenhua CHI660E electrochemical workstation under dark environment. The relative permittivity (ϵ_r) is measured on *Agilent 4294A* under ambient and dark environment at 0.9 V and AC 30 mV (RMS) biased condition with the device structure of ITO/Perovskite/Au.^{5, 6} The water contact angle images were taken on a DSA100 contact angle analysis instrument. XRF was performed by a sequential wavelength-dispersive X-ray fluorescence spectrometer (Shimadzu XRF-1800). The thermogravimetric (TG) analysis is conducted on Discovery TGA550 with a heating rate of 10 °C min⁻¹. The TPV and TPC curves were measured by a platform for all-in-one characterization of solar cells (PAIOS) of FLUXim Company; the pulse length of white light was 1 ms and the background light of 0.1 Sun (10 mW cm⁻²) was applied.

Stability measurement

For the long-term operational stability test, the unencapsulated device of iPA is exposed

to full solar illumination at a bias of 0.95 V. The measurement is performed in a N₂ filled glove box with a cooling system to ensure that the ambient temperature is 20 °C. For the thermal and humidity stability test, the unencapsulated devices or films are stored under corresponding environment. After a certain interval, the J - V curves of these devices are measured and recorded, and the films are subjected to UV-vis absorption measurement or XRD analysis.

TA spectroscopy

Under ambient conditions, the fs-TA measurements were performed on a Helios pump-probe system (Ultrafast Systems LLC) combined with an amplified femtosecond laser system (Coherent). Optical parametric amplifier (TOPAS-800-fs) provided a 600 nm pump pulse (~ 0.2 uJ/pulse at the sample), which was excited by a Ti: sapphire regenerative amplifier (Legend Elite-1K-HE; 800 nm), 35 fs, 7 mJ/pulse, 1 kHz) and seeded with a mode-locked Ti: sapphire laser system (Micra 5) and an Nd: YLF laser (Evolution 30) pumped. Focusing the 800 nm beams (split from the regenerative amplifier with a tiny portion, ~ 400 nJ/pulse) onto a sapphire plate produced the white-light continuum (WLC) probe pulses (420-780 nm and 820-1600 nm). The pulse-to-pulse fluctuation of the WLC is corrected by a reference beam split from WLC. A motorized optical delay line was used to change the time delays (0-8 ns) between the pump and probe pulses. The instrument response function (IRF) was determined to be ~ 100 fs by a routine cross-correlation procedure. A mechanical chopper operated at a frequency of 500 Hz used to modulate the pump pulses such that the fs-TA spectra with and without the pump pulses can be recorded alternately. The temporal and spectral profiles (chirp-corrected) of the pump-induced differential transmission of the WLC probe light (i.e., absorbance change) were visualized by an optical fiber-coupled multichannel spectrometer (with a CMOS sensor) and further processed by the Surface Explorer software. The sample is measured by pump and probe polarizations oriented at the magic angle. A pump pulse with a wavelength of 430 nm was used to excite the perovskite film from the front and back, respectively; the range of the probe beam was 490 nm to 820 nm. According to the signal amplitude of femtosecond visible and near-infrared TA measurements, at least 5 scans were acquired and averaged to obtain a real

data and the high signal-to-noise ratio (SNR) necessary for global analysis.

ToF-SIMS

The time-of-flight secondary-ion mass spectrometry (ToF-SIMS) samples were analyzed in dual beam profiling mode on ToF SIMS 5-100. The primary ion used for analysis was 30 keV Bi³⁺. This ion beam was applied over a 100 μm × 100 μm area at the center of the sputter crater (300 μm × 300 μm). The sputter ion was 5 keV Ar-cluster, a gas cluster ion beam.

¹H NMR

The testing samples in **Figure 3h**, **Figure S10**, and **Figure S11** are fabricated by scraping the 2D perovskite films (10 glasses, 2 cm×2 cm) from the substrate and dissolving it into DMSO-d₆. The sample of “without-PbI₂” in **Figure 3g** is fabricated by dissolving TMAI (4 mg), FAI (5.7 mg), MACl (2.2 mg) into DMSO-d₆ (600 μL). The sample of “with-PbI₂” is obtained by adding PbI₂ (19.1 mg) into the sample of “without-PbI₂”. Therefore, the intensity of H₂O and DMSO with respect to precursors in **Figure 3g** is much weaker than that in **Figure 3h**, **Figure S10**, and **Figure S12**. The ¹H NMR analysis is conducted on Bruker AVANCE III HD 400.

GIWAXS

GIWAXS experiments were performed at beamline BL14B in the Shanghai Synchrotron Radiation Facility (SSRF) with an X-ray wavelength of 0.124 nm. GIWAXS patterns were acquired with a grazing incidence angle of 0.16° and an exposure time of 60 s.

Space-charge limited currents (SCLC)

Electron-only devices are fabricated with structure of ITO/SnO₂/2D perovskite/PCBM/Ag. Hole-only devices are fabricated with structure of ITO/PEDOT:PSS/2D perovskite/Spiro-OMeTAD/Ag. The 2D perovskite layer is iPA or nBA.

The dark *J–V* curves of electron-only devices and hole-only devices are measured under ambient air conditions, with a scan step 0.01 V. The trap density (N_{trap}) can be calculated according to the following formula:

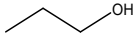
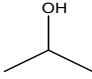
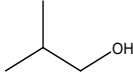
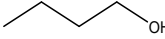
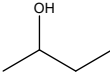
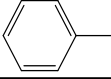
$$N_{trap} = \frac{2\varepsilon_0\varepsilon_r V_{TFL}}{eL^2}$$

In the space-charge limited currents (SCLC) regime, the electron mobilities and the hole mobilities can be estimated via the Mott–Gurney law:

$$\mu = \frac{8J_D L^3}{9\varepsilon_0\varepsilon_r V^2}$$

where e is the electron charge; V_{TFL} is the trap-filled limit voltage; J_D is the current density; L is the film thickness of the perovskite layer; μ is the electron mobility or the hole mobility; ε_r is the relative dielectric constant of the perovskite, The ε_r of iPA is 46.6 and the ε_r of nBA is 47.5, as shown in **Figure S25**; ε_0 is the permittivity of free space (8.85×10^{-12} F m⁻¹); V is the internal voltage in the device.

Table S1 The molecular structure and physicochemical parameter of antisolvents used in this study, and the average apparent grain size of 2D perovskite films prepared by these alcoholic antisolvent.

Structure	Name	Dielectric constant	Viscosity (mPa·s)	Boiling point (T _b /°C)	Average grain size (nm)
	n-propanol	22.2	2.26	97.2	332
	isopropanol	18.3	2.43	82.4	142(fresh) 680(annealed)
	isobutanol	18.0	4.00	107.9	1345
	n-butanol	17.1	2.95	117.7	916
	sec-butanol	15.5	4.21	99.5	1290
	toluene	2.24	0.59	110.6	1972

Note: The viscosity is recorded under 20 °C. The dielectric constant is used to evaluate the polarity. The average apparent grain size is the statistical result of SEM. It is worth noting that the apparent grains may be aggregates of small crystallites with different orientations.

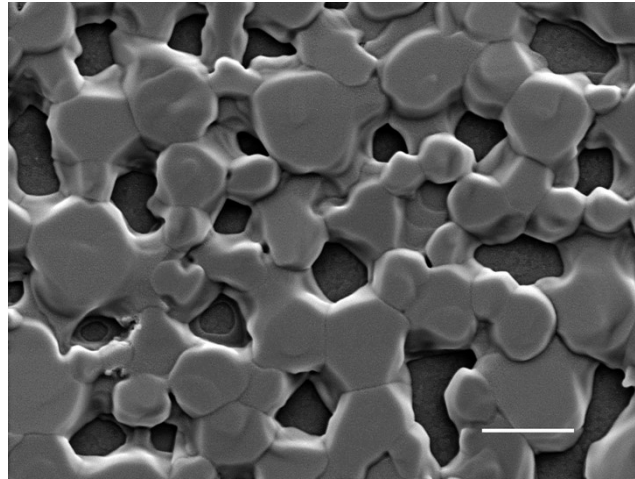


Figure S1 Top view SEM image of 2D perovskite film prepared by toluene; scale bar: 2 μm .

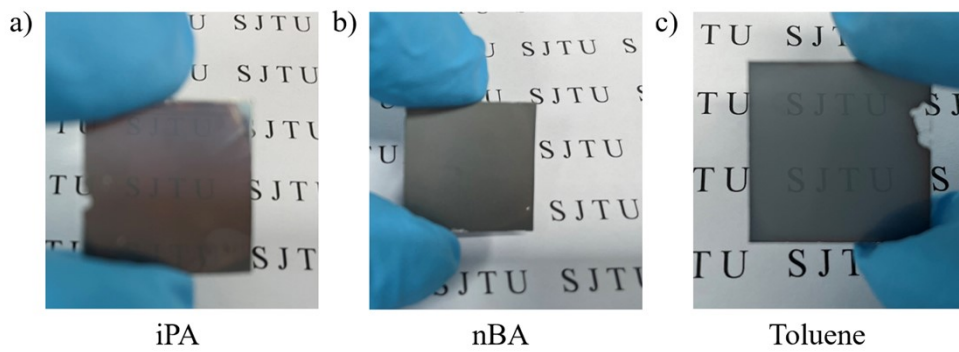


Figure S2 Photographic images of (a) iPA, (b) nBA, and (c) the film prepared by toluene. The side length of glass is 2 cm.

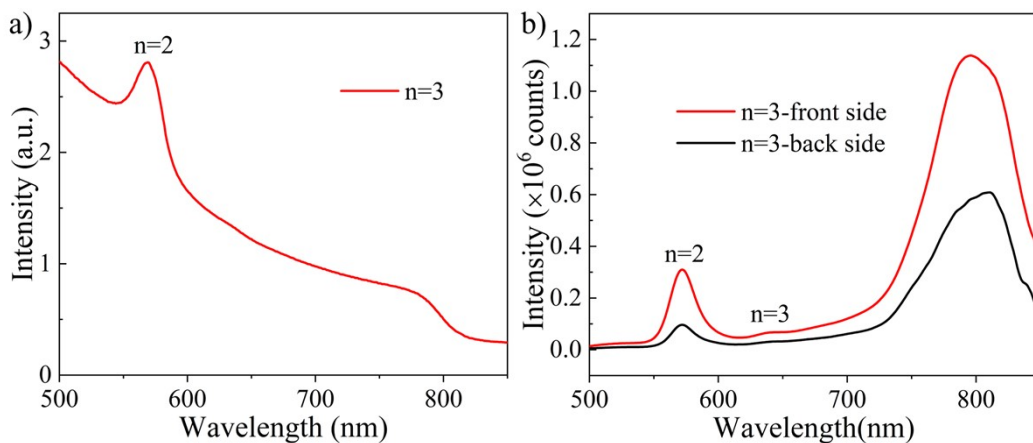


Figure S3 (a) UV-vis absorption spectra of the quasi-2D perovskite film with an average n-value of 3 (precursor solution: TMAI:FAI:PbI₂:MACl=2:2:3:2). (b) PL spectra of the quasi-2D perovskite film of n=3 under front side excitation and back side excitation.

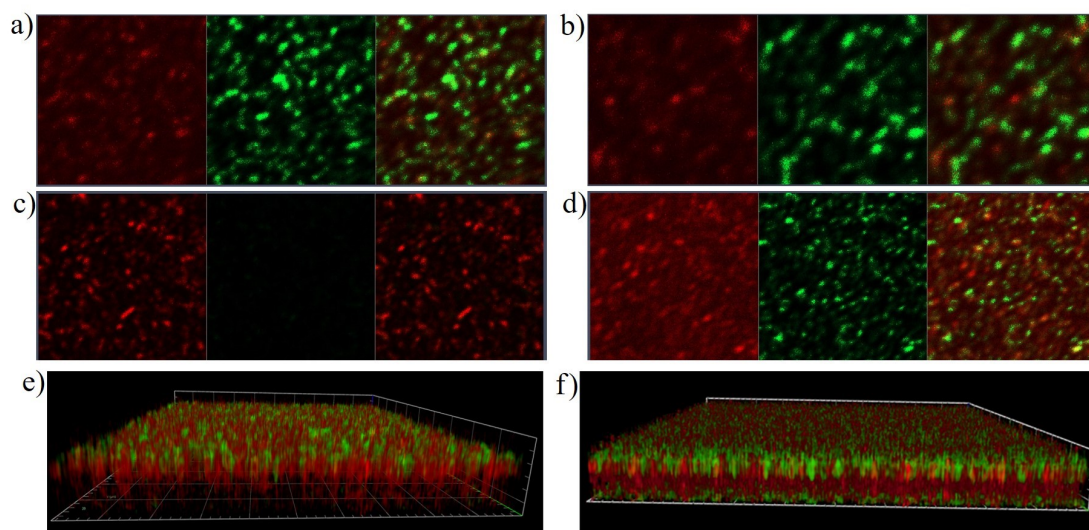


Figure S4 CLSM-PL mapping of iPA and nBA under (a and b) front side excitation and (c and d) back side excitation. In each image of CLSM-PL, three sub images from left to right are 3D-like phase (650-700 nm), low-n-value phase (550-630 nm), and the merge image (550-700 nm). The reconstructed 3D images of (e) iPA and (f) nBA from the CLSM-PL measurement.

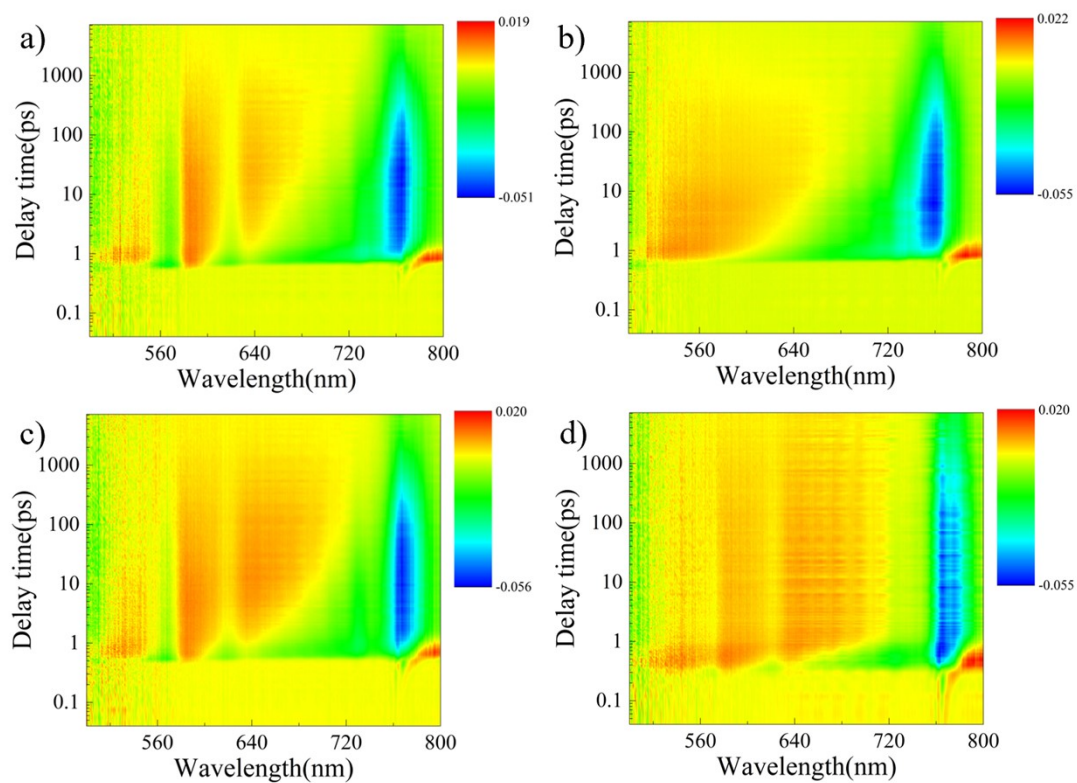


Figure S5 Pseudo color TA spectroscopy images of (a) iPA under front side excitation, (b) iPA under back side excitation, (c) nBA under front side excitation, and (d) nBA under back side excitation.

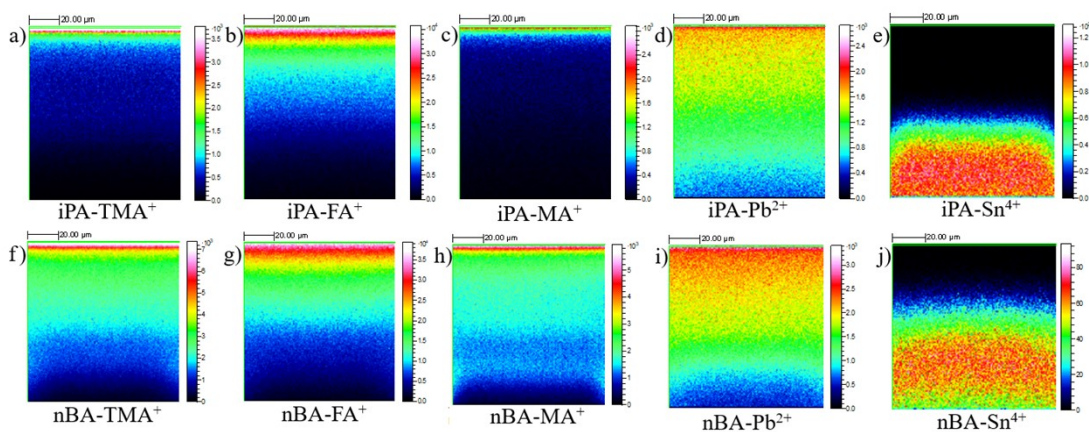


Figure S6 2D images of the depth profile of (a and f) TMA⁺, (b and g) FA⁺, (c and h) MA⁺, (d and i) Pb²⁺, (e and j) Sn⁴⁺ in iPA and nBA, respectively.

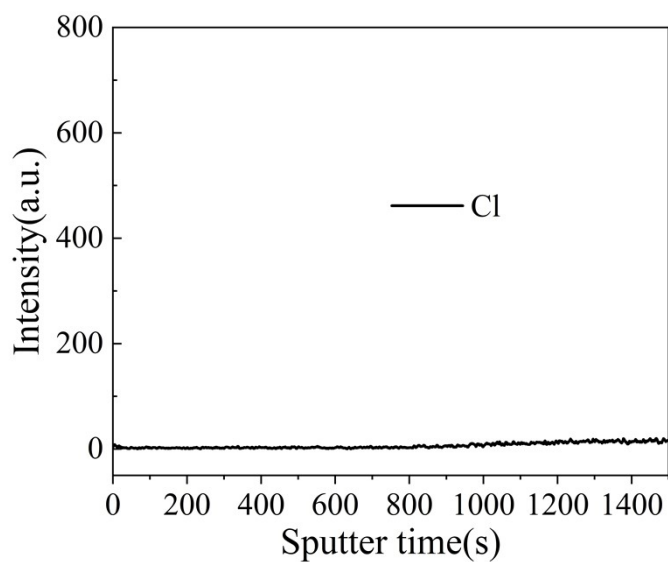


Figure S7 ToF-SIMS depth profile of Cl element in the film of iPA.

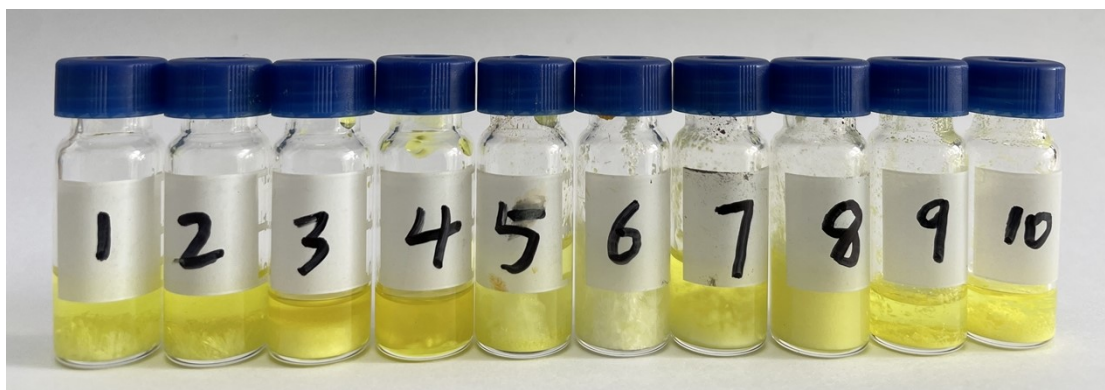


Figure S8 Photographic images of solutions with different organic cations precipitated by iPA and nBA, respectively.

Table S2 Critical volume of antisolvent required to precipitate corresponding solutions.

Number	1#	3#	5#	7#	9#
Composition	FAI+PbI ₂	MAI+PbI ₂	TMAI+PbI ₂	Precursor	PbI ₂
Volume of iPA (μL)	300	100	580	400	80
Number	2#	4#	6#	8#	10#
Volume of nBA (μL)	240	100	540	420	60

Note: the composition of Precursor is TMAI:FAI:PbI₂:MAI=2:4:5:4.

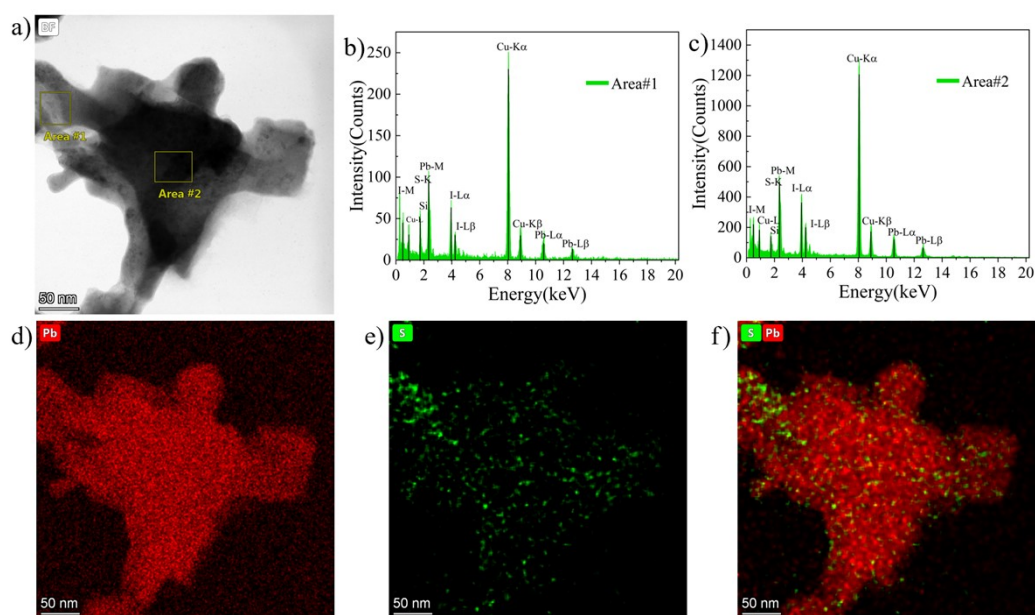


Figure S9 (a) TEM image of iPA under bright filed. The integrated spectra of (b) Area#1 and (c) Area#2 in Figure S9a. The EDS mapping of (d) Pb element, (e) S element, and (f) the merged image of Pb element and S element.

Table S3 Atomic ratio calculated from Figure 9b and Figure 9c.

	Sulfur(S)	Lead (Pb)	Iodine (I)
Area#1	9.2%	28.3%	62.5%
Area#2	0.7%	33.2%	66.1%

Note: The atomic ratio of S element of n=2 phase is 10%, calculated from the structural formula of TMA₂FAPb₂I₇.

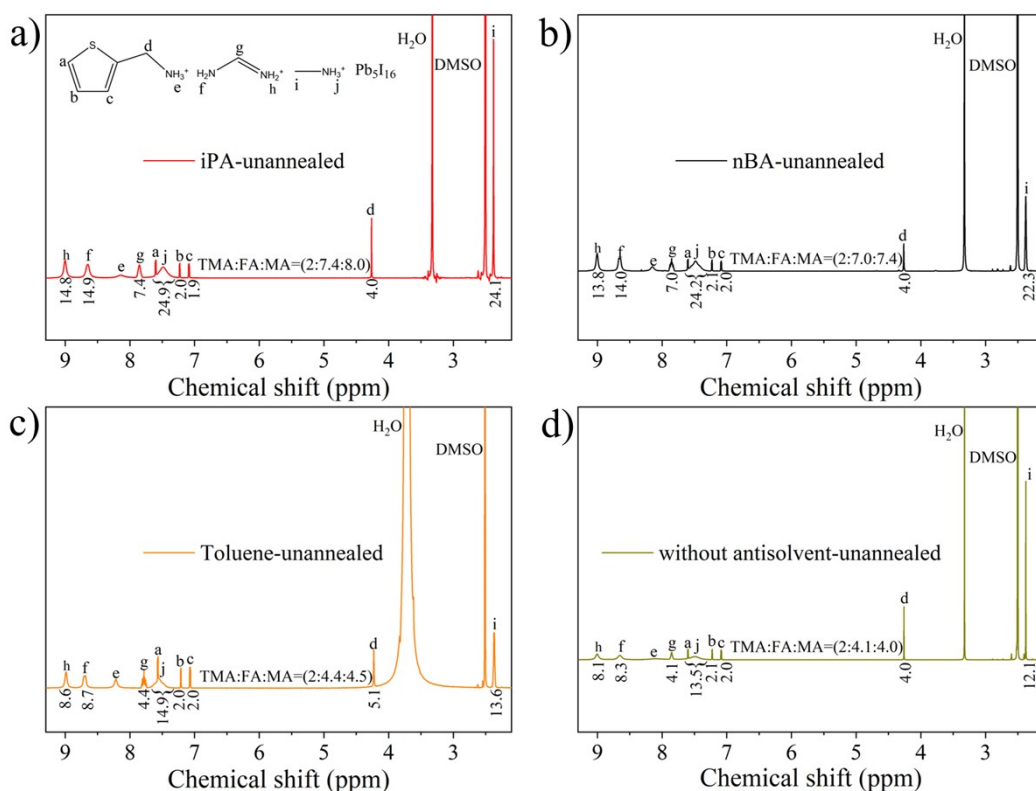


Figure S10 ^1H NMR spectra of unannealed perovskite films deposited by (a) iPA, (b) nBA, (c) toluene, and (d) without antisolvent washing process. The proportion of TMA in iPA-unannealed (2:15.4) and nBA-unannealed (2:14.4) is lower than the film of Toluene-unannealed (2:8.9) and the film without antisolvent washing and without annealing process (2:8.1). This is reasonable considering that the solubility of organic cations in alcoholic solution (iPA and nBA) is much higher than nonpolar solvent (toluene in this study). In addition, the solubility of TMAI is much higher than that of FAI and MAI in iPA and nBA. Details can be seen in the **experiment part** of solubility test.

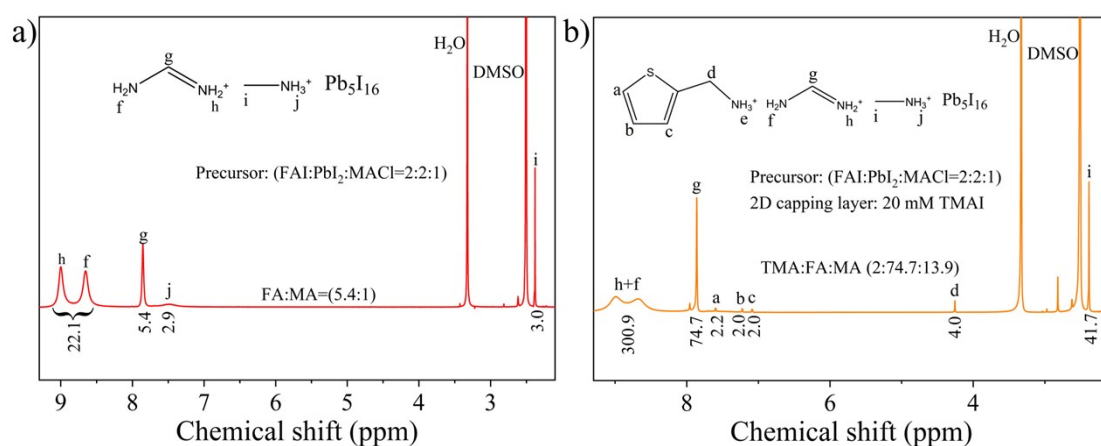


Figure S11 (a) ^1H NMR spectrum of the perovskite film prepared from a precursor solution of $\text{FAI}:\text{PbI}_2:\text{MACl}=2:2:1$, the antisolvent is isopropanol. (b) ^1H NMR spectrum of the film of (a) after depositing a 2D perovskite capping layer (a solution of TMAI (20 mM in isopropanol) was spin coated at 5000 rpm).

Table S4 The relative content of different components in the film.

Sample	TMAI:FAI: PbI ₂ :MACl in precursor	TMA:FA:MA (from ¹ H NMR)	Fraction of TMA (%)	S:Pb:I (from XRF)
iPA	2:4:5:4	2:10.7:6.2	10.6	2:17.5:55.4
nBA		2:9.1:4.9	12.5	2:14.7:46.5
Control (no washing)		2:5.3:1.4	23.0	/
iPA-unannealed		2:7.4:8.0	11.5	
nBA-unannealed		2:7.0:7.4	12.2	
Toluene-unannealed		2:4.4:4.5	18.3	
No washing-unannealed		2:4.1:4.0	19.8	
3D (FA/MA)	0:2:2:1	0:5.4:1	0	
2D/3D (FA/MA)	0:2:2:1+2D capping layer	2:74.7:13.9	2.2	

Note: The fraction of TMA is calculated by the formula of TMA/(TMA+FA+MA) and the molar ratio is used in this table.

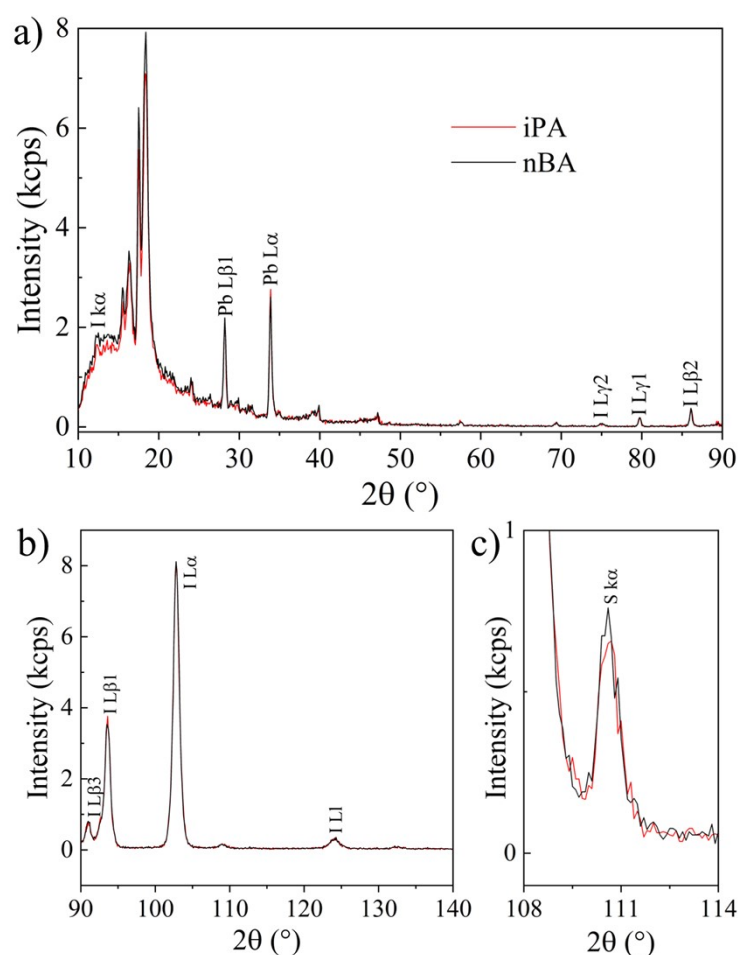


Figure S12 Wavelength-dispersive XRF spectra of iPA and nBA with a wavelength range of (a) 10°-90°, (b) 90°-140°, and (c) 108°-114°.

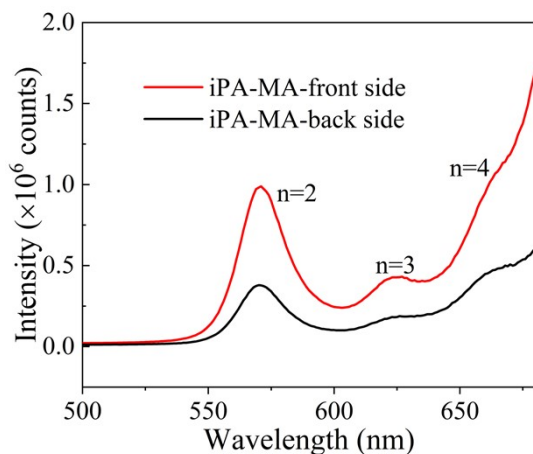


Figure S13 PL spectra of the MA-based quasi-2D perovskite film (iPA-MA) under front side excitation and back side excitation.

Table S5 Champion and average photovoltaic performance of 2D PSCs

2D PSCs	Modes	V_{oc} (V)	FF	J_{sc} (mA cm^{-2})	$J_{sc}(\text{EQE})$ (mA cm^{-2})	PCE(%)
iPA	R/F	1.15/1.15	0.79/0.78	22.15/22.02	21.52	20.12/19.79
	Average	1.14 \pm 0.01	0.75 \pm 0.02	22.00 \pm 0.15		18.81 \pm 0.65
nBA	R/F	1.05/1.01	0.71/0.70	20.85/21.00	20.47	15.54/14.81
	Average	1.04 \pm 0.02	0.67 \pm 0.02	20.65 \pm 0.26		14.39 \pm 0.55

Note: R is the reverse scan mode and F is the forward scan mode. The average photovoltaic parameters are calculated by counting 40 devices.

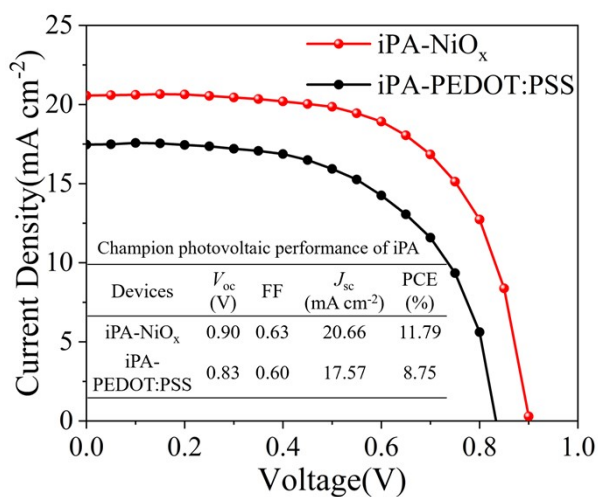


Figure S14 J - V curves of iPA with an inverted device structure.

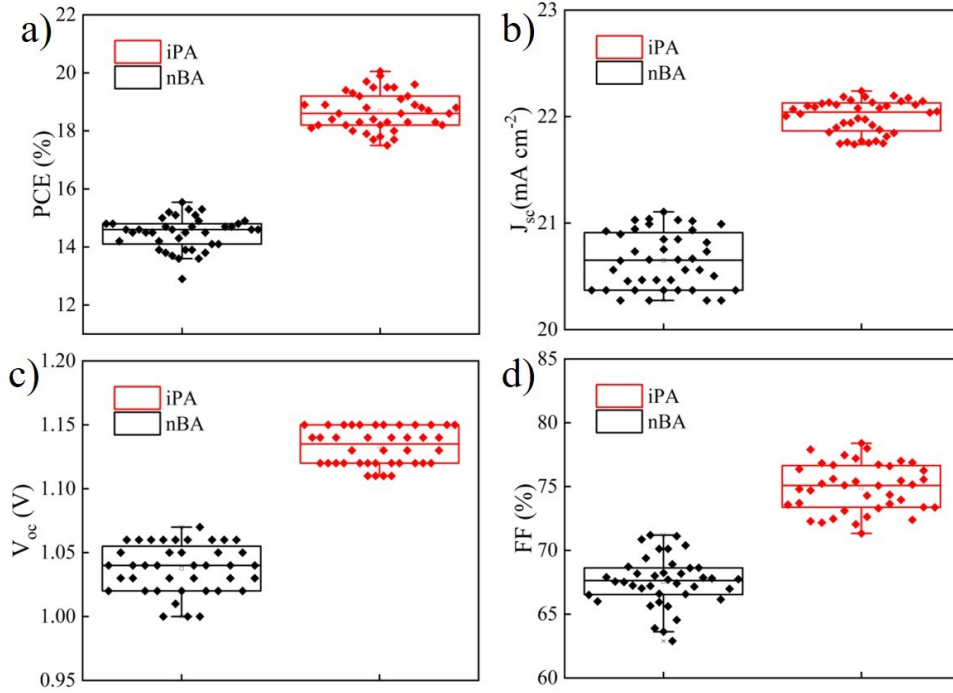
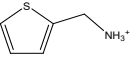
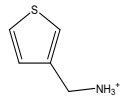
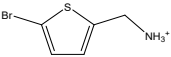
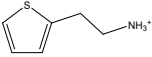
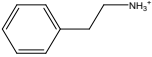
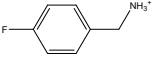
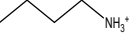


Figure S15 Statistics photovoltaic parameters of iPA and nBA, (a) PCE, (b) J_{sc} , (c) FF, (d) V_{oc} .

Table S6 Champion photovoltaic performance of devices with different spacer cations, the device structure and the fabrication process of 2D perovskite films is the same to that of iPA.

Chemical structure of spacer cations	Abbreviation	V_{oc} (V)	FF	J_{sc} (mA cm^{-2})	PCE(%)
	TMA	1.15	0.79	22.15	20.12
	3TMA	1.14	0.76	21.73	18.83
	BTMA	1.12	0.74	20.85	17.28
	TEA	1.05	0.71	19.23	14.33
	PEA	0.76	0.58	17.64	7.78
	FPMA	0.80	0.63	18.21	9.18
	BA	0.96	0.71	16.58	11.30

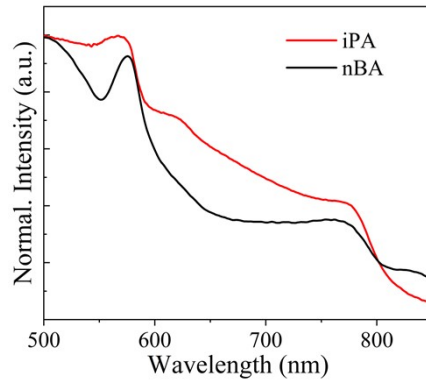


Figure S16 UV-vis absorption spectra of iPA and nBA. The quasi-2D perovskite films are directly exposed to 85%RH for 360 h.

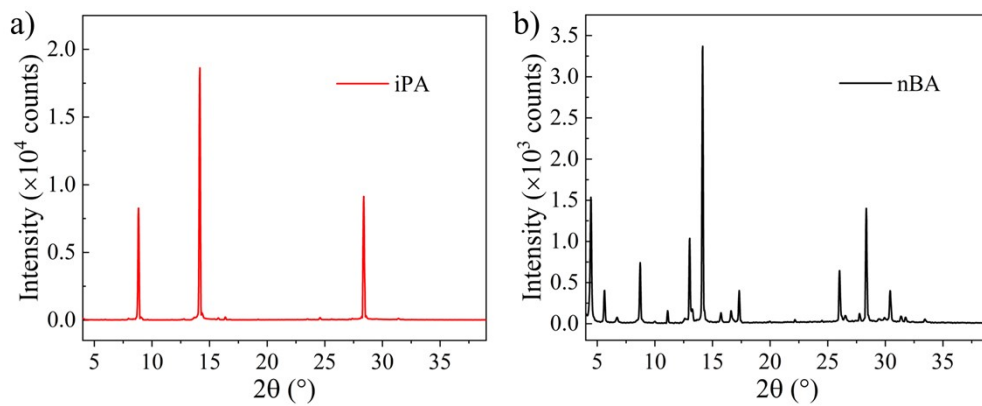


Figure S17 XRD patterns of iPA and nBA. The quasi-2D perovskite films are directly exposed to 85%RH for 360 h.

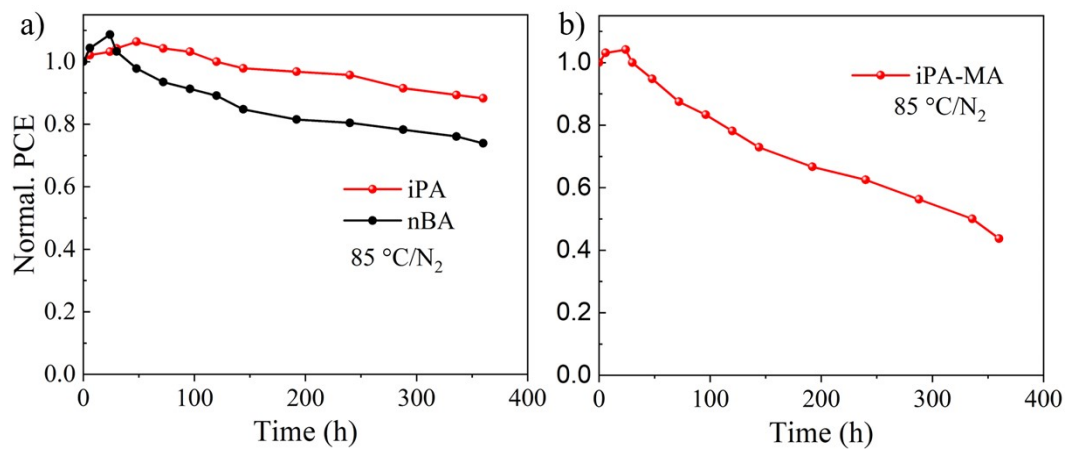


Figure S18 The thermal stability of (a) iPA and nBA, (b) iPA-MA.

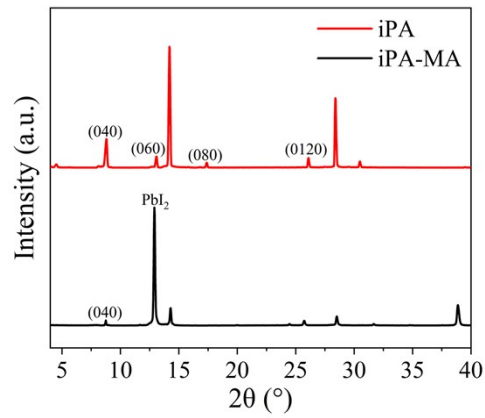


Figure S19 XRD patterns of iPA and iPA-MA. The quasi-2D perovskite films are directly exposed to 85 °C for 360 h.

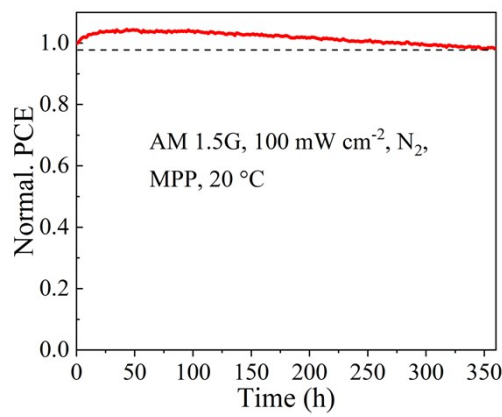


Figure S20 The long-term operational stability of iPA.

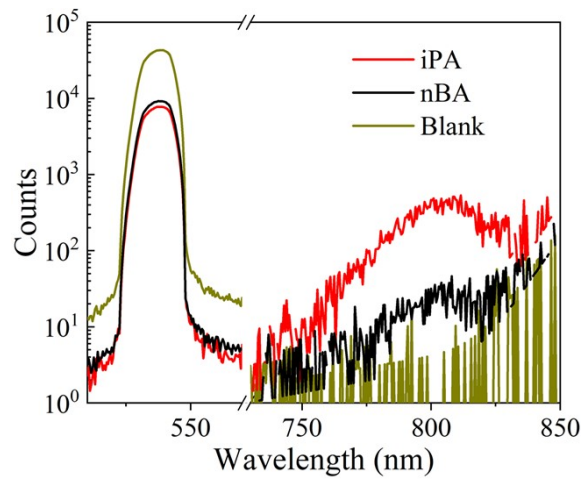


Figure S21 The complete spectra for the measurement of PLQE of iPA, nBA, and blank sample (BaSO_4).

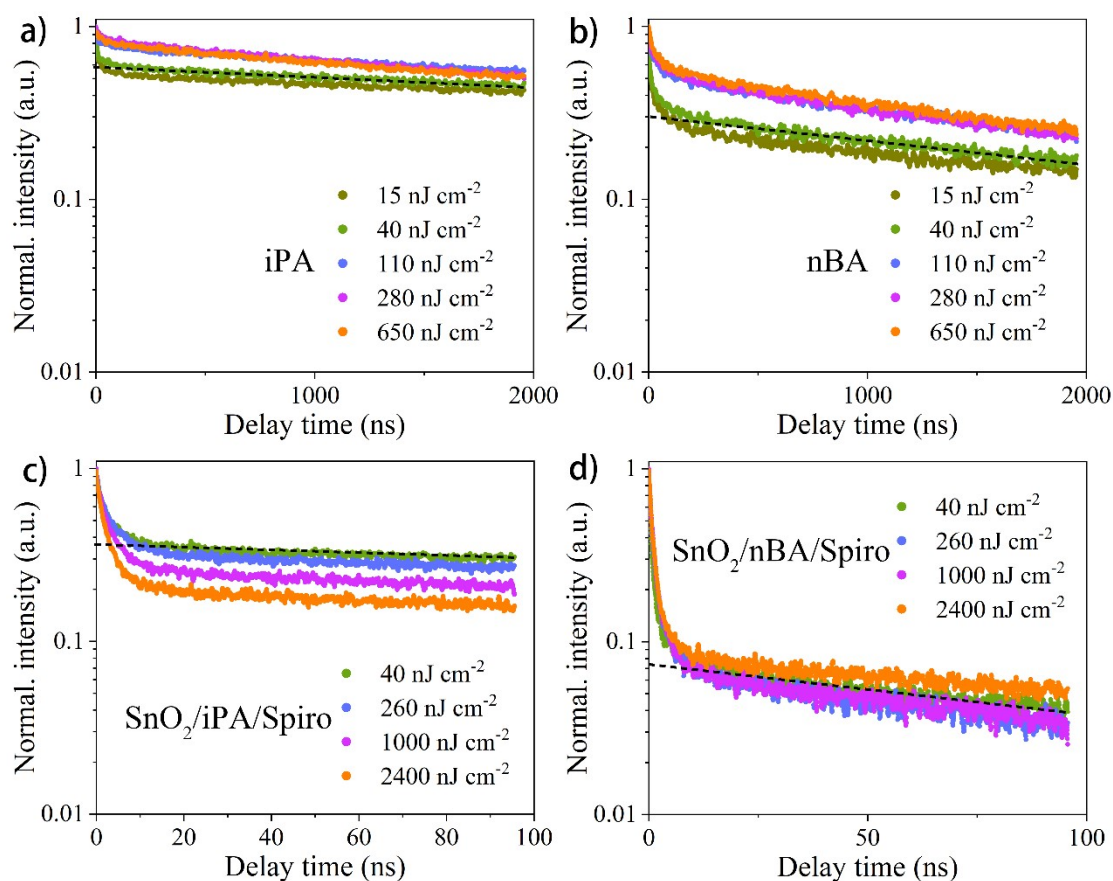


Figure S22 Fluence-dependent TRPL measurements of (a) iPA, (b) nBA, (c) $\text{SnO}_2/\text{iPA}/\text{Spiro}$, and (d) $\text{SnO}_2/\text{nBA}/\text{Spiro}$. The films are excited at 470 nm from the top surface side. The dash lines are extrapolated fits to the mono-exponential tail of TRPL decays at the fluence of 40 nJ cm^{-2} , from which the PL decay time values are obtained.

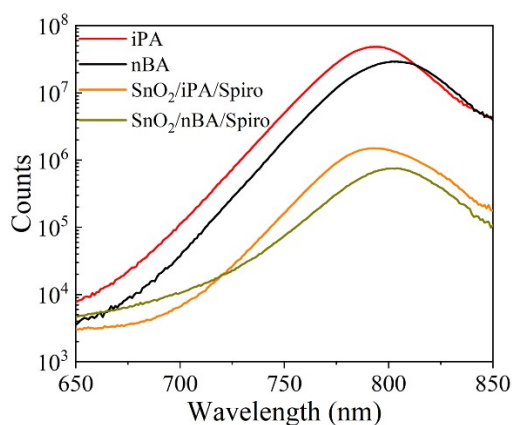


Figure S23 The relative steady-state PL spectra of iPA, nBA, $\text{SnO}_2/\text{iPA}/\text{Spiro}$, and $\text{SnO}_2/\text{nBA}/\text{Spiro}$. The films are excited at 470 nm through the top surface side.

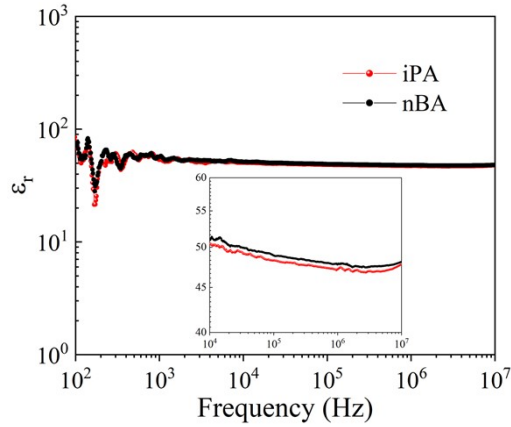


Figure S24 Relative permittivity (ϵ_r) as a function of frequency at dark condition with ITO/Perovskite/Au device structure under 0.9 V and AC 30 mV (RMS) biased condition. The inset is a local enlarged view. The ϵ_r of iPA is 46.6 and the ϵ_r of nBA is 47.5.

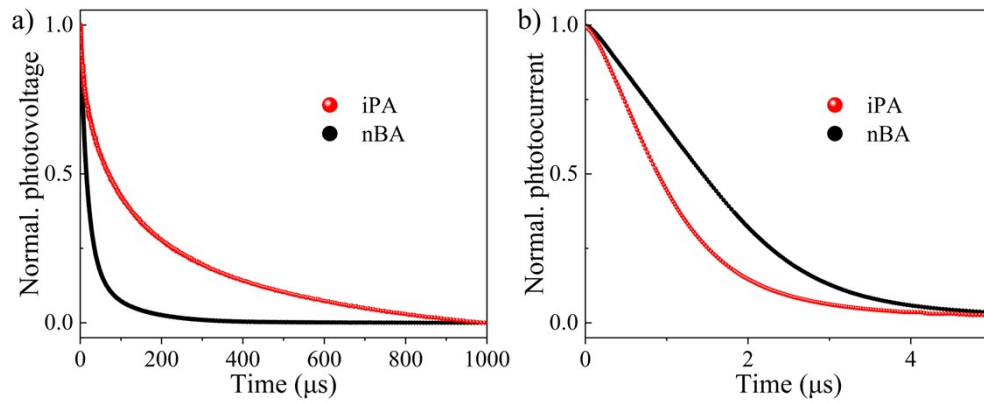


Figure S25 (a) Transient photovoltage and (b) transient photocurrent decay kinetics of iPA and nBA.

Table S7 Fitting parameters of EIS spectra of iPA and nBA.

Devices	$R_s(\Omega)$	R1	C1	R2	C2
iPA	10.00	1.51×10^5	7.66×10^{-7}	8801	2.16×10^{-8}
nBA	13.99	1.72×10^4	1.34×10^{-8}	8857	3.52×10^{-7}

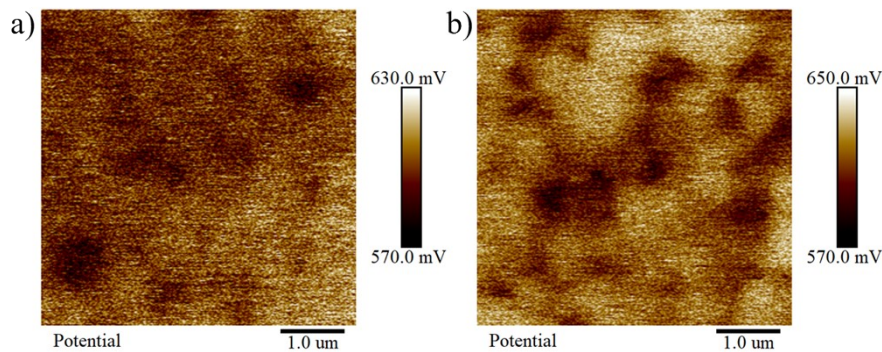


Figure S26 CPD mappings obtained from KPFM measurement of (a) iPA and (b) nBA.

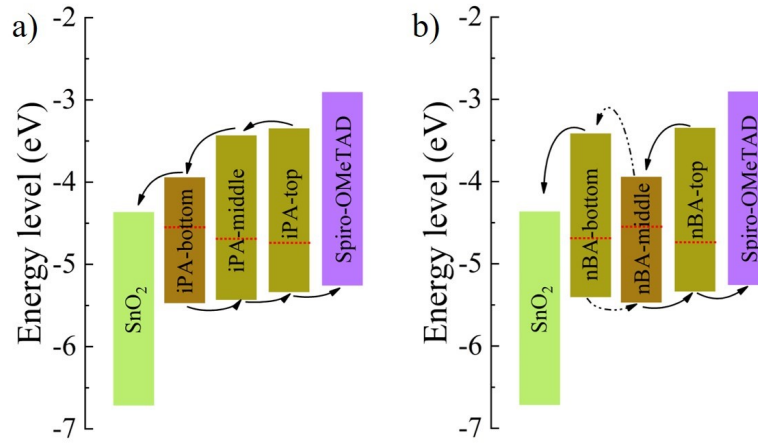


Figure S27 Energy band alignment of iPA and nBA. The red dotted line is the E_F .

Table S8 Energy levels of iPA, nBA, and 3D perovskite films

Sample	Conduction band (eV)	Fermi level (eV)	Valence band (eV)
iPA	~3.37	-4.73	-5.36
nBA	~3.40	-4.68	-5.39
3D	-3.93	-4.53	-5.46

Notes: The Fermi levels and valence band maxima are obtained by UPS. The conduction band minima are obtained by adding the optical bandgaps to the valence band maxima, where the optical bandgap of iPA and nBA is 1.99 eV, and the 3D perovskite is 1.53 eV.

Table S9 Summary of photovoltaic performance and stability of Ruddlesden–Popper phase PSCs

Year	Composition and n-value	PCE(%)	J_{sc} (mA cm ⁻²)	Method	n-value distribution/ device structure	Stability (% of PCE after # of hours at %RH)	Ref
2018	3BBA ₂ MA ₂ Pb ₃ I ₈ Cl ₂ , n=3.3	18.2	18.22	Hot-casting	Normal/Inverted	82%/2400 h/40%RH	7
2019	BA ₂ MA ₃ Pb ₄ I ₁₃ , n=4	17.3	19.86	Hot-casting	Normal/Inverted	95.5%/2000 h/N ₂	8
2020	BA ₂ (MA _{0.8} FA _{0.15} Cs _{0.05}) ₄ Pb ₅ I ₁₆ , n=5	18.0	21.38	Hot-casting	Normal/Inverted	85%/500 h/N ₂ , 60 °C	9
2020	GA _{0.2} BA _{1.8} MA ₅ Pb ₆ I ₁₉ , n=6	18.2	18.71	Hot-casting	Normal/Inverted	90%/1340 h/50±5%RH	10
2020	MTEA ₂ FA ₄ Pb ₅ I ₁₆ , n=5	18.1	21.77	Hot-casting	×/Inverted	87.1%/1000 h/illumination	11
2020	FPEA ₂ MA ₃ Pb ₄ I ₁₃ , n=4	18.1	19.04	Hot-casting	Normal/Inverted	90%/720/40-50%RH	12
2021	AA ₂ MA ₃ Pb ₄ I ₁₃ , n=4	18.4	18.57	Hot-casting	Normal/Inverted	99.3%/1850 h/N ₂	13
2019	FPEA ₂ MA ₄ Pb ₅ I ₁₆ , n=5	17.3	19.00	Additives	Normal/Inverted	93%/500 h/60±5%RH	14
2020	BA ₂ MA ₃ Pb ₄ I ₁₃ , n=4	16.5	18.67	Additives	Normal/Inverted	89%/816 h/55-60%RH	15
2020	PEA ₂ MA ₃ Pb ₄ I ₁₃ , n=4	17.0	18.47	Additives	×/Inverted	92%/3360 h/40%RH	16
2020	PEA ₂ MA ₃ Pb ₄ I ₁₃ , n=4	18.5	18.52	Additives	Normal/Inverted	90%/1200 h/40%RH	17
2021	TBA ₂ MA ₁₉ Pb ₂₀ I ₆₁ , n=20	19.7	23.70	Additives	Normal/Inverted	90%/350 h/N ₂ , illumination	18
2020	isoBA ₂ MA ₄ Pb ₅ I ₁₆ , n=5	16.0	18.10	Blow-drying	Normal/Inverted	90%/500 h/30-40% encapsulated	19
2020	ThMA ₂ FA ₄ Pb ₅ I ₁₆ , n=~5	19.1	23.39	Antisolvent	Normal/Inverted	99%/552 h/30±5%RH	20
2020	BA ₂ MA ₃ Pb ₄ I ₁₃ , n=4	16.2	16.75	Hot-casting	Pure/Normal	93.8%/4680/65±10%RH	21
2019	PEA ₂ MA ₄ Pb ₅ I ₁₆ , n=5	18.0	17.91	Vacuum	Random/Inverted	96.1%/5760 h/N ₂	22
2020	NpMA ₂ MA ₃ Pb ₄ I ₁₃ , n=4	17.2	20.89	Antisolvent	Random/Inverted	89%/1000 h/30±5%RH	23
2019	CMA ₂ MA ₈ Pb ₉ I ₂₈ , n=9	15.0	19.04	Antisolvent	Reverse/Normal	95%/4600 h/40-70%RH	24
2020	isoBA ₂ (Cs _{0.02} MA _{0.64} FA _{0.34}) ₄ Pb ₅ I ₁₆ , n=5	16.0	~21.00	Antisolvent bathing	Reverse/Normal	90%/1500 h/30±10%RH	25
2021	4TFBZA ₂ MA ₅₉ Pb ₆₀ I ₁₈₁ , n=60	17.1	21.66	Antisolvent	Reverse/Normal	84%/1000 h/N ₂	26
2021	TMA ₂ FA _{10.7} MA _{6.2} Pb _{17.5} I _{55.4} , n=18	20.1	22.15	Antisolvent	Reverse/Normal	98%/2000 h/30±5%RH, 96%/360 h/N ₂ , illumination	This work

Notes: It is worth noting that in all work except this study, the composition and n-value in the film are derived from the feed ratio.

References

1. A. H. Proppe, R. Quintero-Bermudez, H. Tan, O. Voznyy, S. O. Kelley and E. H. Sargent, *J Am Chem Soc*, 2018, **140**, 2890-2896.
2. M. Kim, G. H. Kim, T. K. Lee, I. W. Choi, H. W. Choi, Y. Jo, Y. J. Yoon, J. W. Kim, J. Lee, D. Huh, H. Lee, S. K. Kwak, J. Y. Kim and D. S. Kim, *Joule*, 2019, **3**, 2179-2192.
3. J. Liang, Z. Zhang, Y. Zheng, X. Wu, J. Wang, Z. Zhou, Y. Yang, Y. Huang, Z. Chen and C.-C. Chen, *Journal of Materials Chemistry A*, 2021, **9**, 11741-11752.
4. J. C. de Mello, H. F. Wittmann and R. H. Friend, *Advanced Materials*, 1997, **9**, 230-232.
5. L. Wang, X. Wang, L. Zhu, S.-B. Leng, J. Liang, Y. Zheng, Z. Zhang, Z. Zhang, X. Liu, F. Liu and C.-C. Chen, *Chemical Engineering Journal*, 2022, **430**, 132730.
6. H. Kim, S.-U. Lee, D. Y. Lee, M. J. Paik, H. Na, J. Lee and S. I. Seok, *Advanced Energy Materials*, 2019, **9**, 1902740.
7. R. Yang, R. Li, Y. Cao, Y. Wei, Y. Miao, W. L. Tan, X. Jiao, H. Chen, L. Zhang, Q. Chen, H. Zhang, W. Zou, Y. Wang, M. Yang, C. Yi, N. Wang, F. Gao, C. R. McNeill, T. Qin, J. Wang and W. Huang, *Advanced Materials*, 2018, **30**, 1804771.
8. G. Wu, X. Li, J. Zhou, J. Zhang, X. Zhang, X. Leng, P. Wang, M. Chen, D. Zhang, K. Zhao, S. Liu, H. Zhou and Y. Zhang, *Advanced Materials*, 2019, **31**, 1903889.
9. X. Li, G. Wu, M. Wang, B. Yu, J. Zhou, B. Wang, X. Zhang, H. Xia, S. Yue, K. Wang, C. Zhang, J. Zhang, H. Zhou and Y. Zhang, *Advanced Energy Materials*, 2020, **10**, 2001832.
10. X. Lian, H. Wu, L. Zuo, G. Zhou, X. Wen, Y. Zhang, G. Wu, Z. Xie, H. Zhu and H. Chen, *Advanced Functional Materials*, 2020, **30**, 2004188.
11. H. Ren, S. Yu, L. Chao, Y. Xia, Y. Sun, S. Zuo, F. Li, T. Niu, Y. Yang, H. Ju, B. Li, H. Du, X. Gao, J. Zhang, J. Wang, L. Zhang, Y. Chen and W. Huang, *Nature Photonics*, 2020, **14**, 154-163.
12. Z. Wang, Q. Wei, X. Liu, L. Liu, X. Tang, J. Guo, S. Ren, G. Xing, D. Zhao and Y. Zheng, *Advanced Functional Materials*, 2021, **31**, 2008404.
13. G. Wu, T. Yang, X. Li, N. Ahmad, X. Zhang, S. Yue, J. Zhou, Y. Li, H. Wang, X. Shi, S. Liu, K. Zhao, H. Zhou and Y. Zhang, *Matter*, 2021, **4**, 582-599.
14. J. Shi, Y. Gao, X. Gao, Y. Zhang, J. Zhang, X. Jing and M. Shao, *Advanced Materials*, 2019, **31**, 1901673.
15. J. Song, G. Zhou, W. Chen, Q. Zhang, J. Ali, Q. Hu, J. Wang, C. Wang, W. Feng, A. B. Djurišić, H. Zhu, Y. Zhang, T. Russell and F. Liu, *Advanced Materials*, 2020, **32**, 2002784.
16. Y. Yang, C. Liu, A. Mahata, M. Li, C. Roldán-Carmona, Y. Ding, Z. Arain, W. Xu, Y. Yang, P. A. Schouwink, A. Züttel, F. De Angelis, S. Dai and M. K. Nazeeruddin, *Energy & Environmental Science*, 2020, **13**, 3093-3101.
17. Y. Yang, C. Liu, O. A. Syzgantseva, M. A. Syzgantseva, S. Ma, Y. Ding, M. Cai, X. Liu, S. Dai and M. K. Nazeeruddin, *Advanced Energy Materials*, 2021, **11**, 2002966.
18. N. Zhou, Y. Zhang, Z. Huang, Z. Guo, C. Zhu, J. He, Q. Chen, W. Sun and H. Zhou, *ACS Nano*, 2021, **15**, 8350-8362.
19. C. Zuo, A. D. Scully, W. L. Tan, F. Zheng, K. P. Ghiggino, D. Vak, H. Weerasinghe, C. R. McNeill, D. Angmo, A. S. R. Chesman and M. Gao, *Communications Materials*, 2020, **1**, 33.
20. H. Lai, D. Lu, Z. Xu, N. Zheng, Z. Xie and Y. Liu, *Advanced Materials*, 2020, **32**, 2001470.
21. C. Liang, H. Gu, Y. Xia, Z. Wang, X. Liu, J. Xia, S. Zuo, Y. Hu, X. Gao, W. Hui, L. Chao, T. Niu, M. Fang, H. Lu, H. Dong, H. Yu, S. Chen, X. Ran, L. Song, B. Li, J. Zhang, Y. Peng, G. Shao,

- J. Wang, Y. Chen, G. Xing and W. Huang, *Nature Energy*, 2021, **6**, 38-45.
22. J. Zhang, J. Qin, M. Wang, Y. Bai, H. Zou, J. K. Keum, R. Tao, H. Xu, H. Yu, S. Haacke and B. Hu, *Joule*, 2019, **3**, 3061-3071.
23. Z. Xu, D. Lu, F. Liu, H. Lai, X. Wan, X. Zhang, Y. Liu and Y. Chen, *ACS Nano*, 2020, **14**, 4871-4881.
24. Y. Wei, H. Chu, Y. Tian, B. Chen, K. Wu, J. Wang, X. Yang, B. Cai, Y. Zhang and J. Zhao, *Advanced Energy Materials*, 2019, **9**, 1900612.
25. G. Jang, S. Ma, H.-C. Kwon, S. Goh, H. Ban, J. S. Kim, J.-H. Kim and J. Moon, *ACS Energy Letters*, 2020, **6**, 249-260.
26. D. Li, Z. Xing, L. Huang, X. Meng, X. Hu, T. Hu and Y. Chen, *Advanced Materials*, 2021, **n/a**, 2101823.